GFZ
Helmholtz-Zentrum
POTSDAM

HELMHOLTZ-ZENTRUM POTSDAM
DEUTSCHES
GEOFORSCHUNGSZENTRUM

Zhu, Y., Diao, F., Wang, R., Hao, M., Shao, Z., Xiong, X. (2022): Crustal Shortening and Rheological Behavior Across the Longmen Shan Fault, Eastern Margin of the Tibetan Plateau. - Geophysical Research Letters, 49, 11, e2022GL098814.

https://doi.org/10.1029/2022GL098814

Institional Repository GFZpublic: https://gfzpublic.gfz-potsdam.de/

Check for updates

Geophysical Research Letters

RESEARCH LETTER
10.1029/2022GL098814

Crustal Shortening and Rheological Behavior Across the Longmen Shan Fault, Eastern Margin of the Tibetan Plateau

Yage Zhu[1], Faqi Diao[1], Rongjiang Wang[1,2], Ming Hao[3], Zhigang Shao[4], and Xiong Xiong[1]

[1]Hubei Subsurface Multi-Scale Imaging Key Laboratory, Institute of Geophysics and Geomatics, China University of Geosciences, Wuhan, China, [2]GFZ German Research Centre for Geosciences, Potsdam, Germany, [3]Second Monitoring and Application Center, China Earthquake Administration, Xi'an, China, [4]Institute of Earthquake Forecasting, China Earthquake Administration, Beijing, China

Key Points:

- High lower crustal viscosities ($>10^{21}$ Pa · s) beneath the Longmen Shan fault are required to model the interseismic deformation
- Stress-dependent rheological behavior can reconcile the viscosity evolution during an earthquake cycle
- Earthquake cycle deformation model indicates a higher fault shortening rate than previously estimated

Supporting Information:

Supporting Information may be found in the online version of this article.

Correspondence to:

F. Diao,
fqdiao@cug.edu.cn

Citation:

Zhu, Y., Diao, F., Wang, R., Hao, M., Shao, Z., & Xiong, X. (2022). Crustal shortening and rheological behavior across the Longmen Shan fault, eastern margin of the Tibetan Plateau. *Geophysical Research Letters*, *49*, e2022GL098814. https://doi.org/10.1029/2022GL098814

Received 26 MAR 2022
Accepted 17 MAY 2022

© 2022. American Geophysical Union. All Rights Reserved.

Abstract Knowledge of lithospheric rheology can provide fundamental insights into crustal deformation near the Longmen Shan fault (LMSF). Based on viscoelastic deformation models constrained by interseismic geodetic observations, we obtain an optimal crustal shortening rate of 4.8 ± 0.4 mm/a across the LMSF and an upper mantle viscosity of $5.0 \times 10^{20-21}$ Pa · s beneath eastern Tibet. More importantly, we find a high-viscosity zone ($>10^{21}$ Pa · s) in the lower crust beneath the LMSF, where the steady-state viscosity is significantly higher than the transient viscosity derived from postseismic deformation. Further investigations with a power-law rheology suggest that, due to the stress loading of the Wenchuan earthquake and the relaxation afterwards, the effective lower crustal viscosity decreases to $\sim 10^{18}$ Pa · s immediately after the earthquake and finally recovers to interseismic level ($\sim 10^{21}$ Pa · s). Our results highlight the stress-dependent behavior and the viscoelastic effect of rheological structure beneath the LMSF during the earthquake cycle.

Plain Language Summary Cross-fault crustal deformation derived from geodetic measurements reflects the combined effects of fault motion and lithospheric viscoelastic relaxation, thus can provide important constraints on fault mechanisms and rock rheology. The Longmen Shan fault (LMSF) absorbs the eastern extrusion of the Tibetan Plateau and produces large earthquakes, including the 2008 M_w 7.9 Wenchuan earthquake. Previous studies mostly used elastic models to infer slip parameters of the LMSF, which may bias the parameter estimations and provide no constraint on lithospheric rheological structure. Here we use viscoelastic deformation models and geodetic observations to probe the rheological structure and the crustal shortening rate near the LMSF. Our viscoelastic models suggest that a high lower crustal viscosity ($>10^{21}$ Pa · s) beneath the LMSF is required on the time scale of earthquake cycles ($\sim 10^4$ yrs), in contrast with the low viscosities ($\sim 10^{18}$ Pa · s) inferred from transient postseismic deformation. In-depth analysis with a power-law rheology indicates that the lower crustal viscosity varies temporally as stress evolution after coseismic ruptures. This result may reconcile the discrepancies among viscosities derived from different geophysical observations. Our findings highlight that we may not use the transient postseismic viscosity to represent the stable rheological behavior.

1. Introduction

The Longmen Shan fault (LMSF), site of the 2008 M_w 7.9 Wenchuan earthquake and the 2013 M_w 6.6 Lushan earthquake, defines the eastern margin of the Tibetan Plateau with great topographic relief (Burchfiel et al., 2008; Hubbard & Shaw, 2009; Figure 1). Insights into the lithospheric rheology of this region are of great importance when trying to understand the tectonic evolution and geodynamics, such as the mountain building process and crustal shortening between rigid blocks (Bürgmann & Dresen, 2008). To probe both the rheological structures and properties beneath this region, many studies relying on postseismic deformation, seismic and magnetotelluric imaging have been carried out (e.g., Bao et al., 2020; Diao et al., 2018; Liu et al., 2014; Wang et al., 2021; Zhao et al., 2012).

In order to explain the short-term (months to years) geodetic observations following the Wenchuan earthquake, postseismic deformation studies suggested a weak lower crust with effective viscosities around $\sim 10^{18}$ Pa · s beneath the eastern margin of Tibet (e.g., Diao et al., 2018; Huang et al., 2014; Wang et al., 2021). However, seismological and magnetotelluric studies revealed a stable zone of high seismic velocity and high resistivity at a depth of ~40 km west of the LMSF (Bao et al., 2020; Liu et al., 2014; Zhao et al., 2012), which may imply

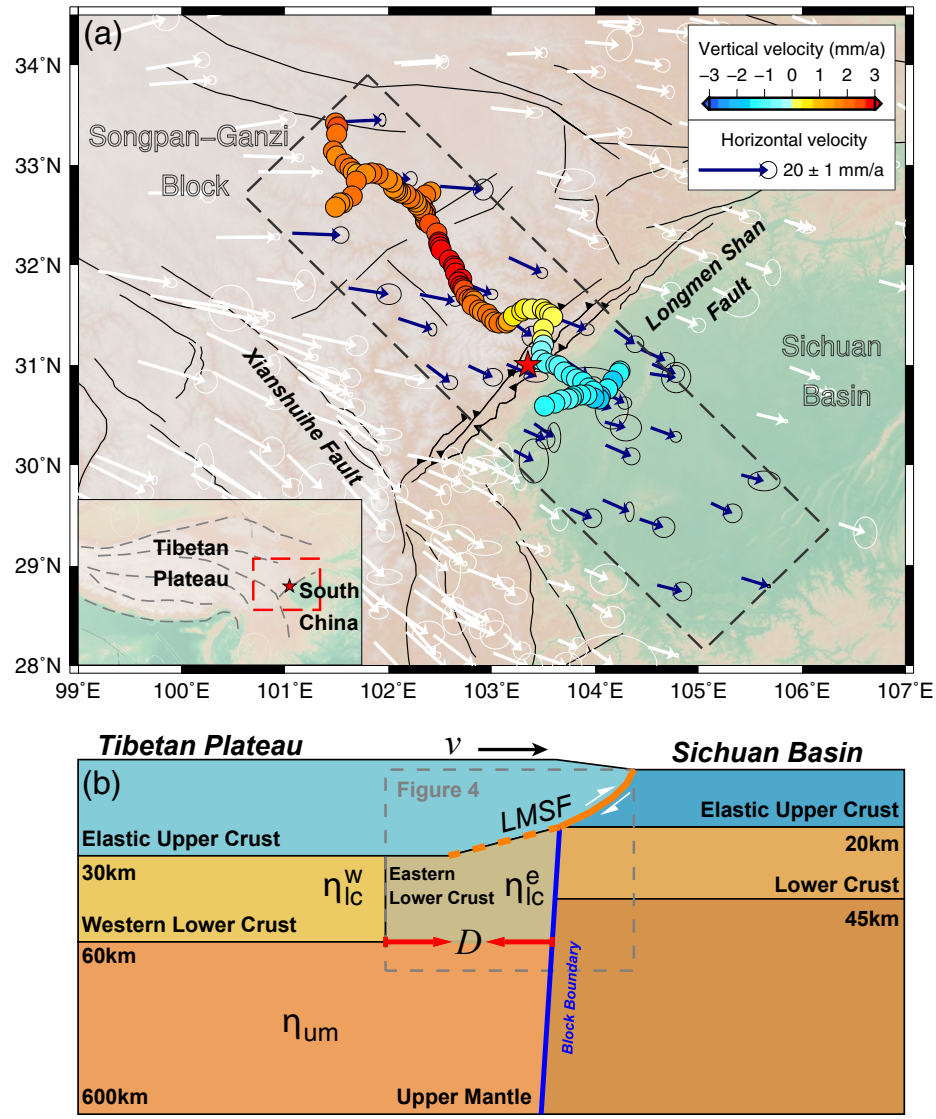

Figure 1. Tectonic setting of the Longmen Shan fault area. The inset shows the location of the study area (red dashed rectangle), and the red star represents the epicenter of the 2008 Wenchuan earthquake. (a) In the main figure, the black dashed rectangle is used to select the velocity measurements. Colored circles represent vertical velocities from leveling measurements (Hao et al., 2014). White vectors represent horizontal GPS velocities with 95% confidence interval relative to the Eurasian plate (Zheng et al., 2017), and the blue vectors in the dashed rectangular are used to build the velocity profile. (b) Sketch map of the structure model across the Longmen Shan fault (LMSF). The orange curve indicates the fault locking area with a variable dip angle, instead of a uniform angle in previous simplified geometry, and the dashed curve indicates the detachment. The blue curve delineates the block boundary between Tibet and Sichuan Basin. *D* indicates the lateral extension of the eastern lower crust beneath Tibet.

materials of high strength and high viscosity. Clark and Royden (2000) proposed a lower crustal flow model to explain the large topographic relief across the LMSF, and suggested that a high lower crustal viscosity of $\sim 10^{21}$ Pa · s is required to sustain the high topography west of the LMSF. These results may reflect viscosities under different stress states across different time scales, for example, transient stress adjustment on short time scale (yrs) and steady stress loading on large time scale ($\sim 10^6$ yrs). In order to reconcile the viscosities inferred from different investigations, further studies on the rheological behavior, especially that on the time scale between the transient postseismic period and the long-term tectonic process, are indispensable. During the interseismic period of earthquake cycles ($\sim 10^4$ yrs), the stress accumulated by fault locking is partially relaxed by slow viscous flow of the ductile lower crust and upper mantle, leading to observable surface deformation (Savage & Prescott, 1978; Wang et al., 2012). Based on the newly developed models that include viscoelastic effects

during earthquake cycles, we can explore the long-term viscosity with interseismic geodetic observation (Diao et al., 2019, 2021; Li et al., 2020; Wang et al., 2012).

Interseismic geodetic observation also plays a vital role in probing kinematic fault parameters, which are fundamental to understanding seismogenic mechanism and associated seismic hazard assessments (Meade, 2007; Burchfiel et al., 2008; P. Zhang et al., 2010). Previous investigations suggested low crustal shortening rates of 0–3 mm/a (e.g., Chen et al., 2000; Shen et al., 2005; Thatcher, 2007; Zheng et al., 2017), but other competing results proposed shortening rates of 5–6 mm/a (Thompson et al., 2015; Wang & Shen, 2020). These studies used elastic models and neglected the viscoelastic relaxation effects induced by stress accumulation and release during earthquake cycles, which may bias the estimation of kinematic parameter, such as fault slip rate and locking depth (Diao et al., 2019, 2021; Li et al., 2020). Besides, only horizontal deformation rates were used by these previous studies. In fact, the central-southern segment of the LMSF is dominated by thrusting, which would be more sensitive to vertical displacement component.

Here we use the combined observations of horizontal and vertical velocities in the LMSF region to explore the long-term lithospheric rheological structure and the shortening rate across the LMSF based on a viscoelastic earthquake-cycle deformation (VECD) model. With a finite element modeling method, we consider a more realistic fault geometry and lateral variations in the earth structure. Based on the inferred long-term lower crustal viscosity, we further investigate its stress-dependent behavior and temporal variation during an earthquake cycle.

2. Geodetic Observations Across the Longmen Shan Fault

In this study, we build a velocity profile across the southern segment of the LMSF (Figure 1a), along which both vertical and horizontal surface velocities are available. The vertical displacement rates are derived from high-precision leveling observations (Hao et al., 2014). The leveling route across the LMSF was measured 3 times in 1975, 1983, and 1997 by the National Administration of Surveying, Mapping and Geoinformation of China, respectively. The three sessions of measurements were conducted in the first-order leveling, and the standard error for 1 km is less than 1 mm. In order to mitigate the systematic errors accumulated over long leveling routes and provide a regional reference frame for leveling vertical rates, vertical rates of GPS stations were used as *a-priori* constraints, and were combined with leveling observations to infer vertical rates of benchmarks through linear dynamic adjustment (Hao et al., 2014). The leveling measurements capture an obvious uplift (∼3 mm/a) of the eastern Tibetan Plateau (upper panel) relative to the Sichuan Basin (Figure 2).

Besides the vertical velocity measurements, we use the interseismic horizontal GPS velocities provided by Zheng et al. (2017) as additional constraints on our models. They processed the GPS observations collected by the Crustal Movement Observation Network of China-I/II project, and obtained a most complete and up-to-data interseismic horizontal velocity field across the Longmen Shan area based on observations acquired before the Wenchuan earthquake. We select GPS stations within the designed profile (Figure 1a), and project the horizontal velocities onto the fault-perpendicular direction. As shown in Figure 2, these fault-perpendicular horizontal velocities decrease gradually from northwest to southeast, revealing crustal shortening across the fault.

3. Modeling and Methods

3.1. Viscoelastic Earthquake-Cycle Deformation Model

According to the elastic rebound theory (Reid, 1910), accumulated elastic stress on a fault during the interseismic period is released by seismic slip during the rupture, and is rebuilt by fault locking, leading to interseismic surface deformation across the fault. In order to probe the fault slip rate and locking depth, the "back-slip model" was proposed based on elastic and viscoelastic models, respectively (Savage, 1983). The elastic model assumes a steady-state deformation pattern during interseismic periods, and is widely used owing to the simple formulation and reasonable explanation of the observations. The viscoelastic model, which incorporates the viscoelastic relaxation effects driven by stress changes during earthquake cycles, can predict time-dependent interseismic deformation (e.g., Diao et al., 2019; Li et al., 2020; Savage & Prescott, 1978; Wang et al., 2012).

To quantify viscoelastic relaxation throughout an earthquake cycle, Diao et al. (2019) developed a VECD model in a kinematic pattern, in which the interseismic crustal velocity (V) is represented by,

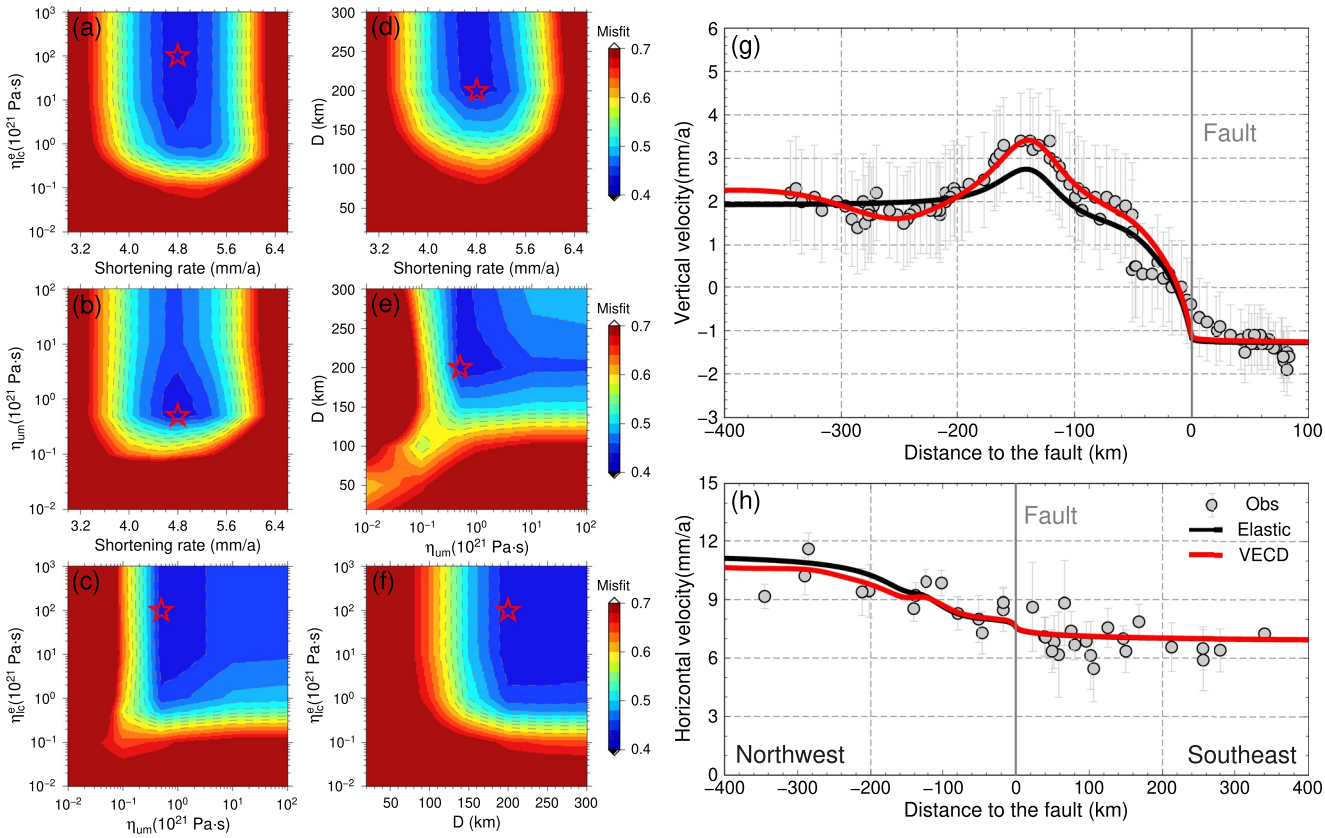

Figure 2. (a–f) represent 4D misfit variance on the (v vs. ηlc), (v vs. η_{um}), (η_{um} vs. η^e_{lc}), (v vs. D), (η_{um} vs. D), and (D vs. η^e_{lc}) transects from viscoelastic earthquake-cycle deformation (VECD) models, respectively. The red stars indicate the optimal values of the parameters. (g and h) are the best data-fittings of the vertical and horizontal velocities, respectively. The red and black curves are predictions of the optimal VECD model and elastic model, respectively. Gray dots with error bar show the surface velocities perpendicular to the fault (95% confidence interval).

$$V(\boldsymbol{x},t) = [v(\boldsymbol{x}) - v_b C(\boldsymbol{x})] + v_b \left[T \sum_{n=0}^{N-1} \frac{\partial}{\partial t} P(\boldsymbol{x}, t - t_0 + nT) - P(\boldsymbol{x},t) \right], \quad (1)$$

where $\boldsymbol{x}$ is the position of the observations, t is the time since the earliest earthquake, N is the number of the past cycles indexed with n, t_0 is the occurrence time of the latest earthquake ($n = 0$), and T is the recurrence interval of the periodic event. v represents the stable crustal velocity due to the relative motion of rigid blocks, and in the present case, v is the shortening rate between the eastern Tibetan Plateau and the Sichuan Basin. v_b is the fault back-slip rate determined by $v_b = v/\cos\delta$, where δ is fault dip angle (McCaffrey et al., 2002; Meade & Hager, 2005). $C(\boldsymbol{x})$ and $P(\boldsymbol{x}, t)$ are the elastic and the viscous part of the displacement Green's function related to fault slip (Diao et al., 2019). $P(\boldsymbol{x}, t)$ is the function of the viscosity of ductile layers. The first and second terms on the right side of Equation 1 represent the elastic and viscous deformation components, respectively, induced by the periodic fault rupture and continuous fault locking. The predicted ground velocity is mainly determined by the shortening rate (v) and the viscosities of ductile layers in the model.

3.2. Model Configurations

By using the finite element code PyLith (Aagaard et al., 2013), we build a 2D VECD model, in which cross-fault variation of the Earth structure and topography are carefully considered. Detailed fault geometric setting with a listric shallow part and a deep sub-horizontal detachment is shown in Figure S1 in Supporting Information S1 (Shen et al., 2009; Wang et al., 2011; Xu et al., 2010). The fault is assumed to be completely locked during interseismic periods following Thompson et al. (2015), and the slip-deficit accumulated since the last earthquake is released in a periodic rupture. The recurrence interval (T) is assumed to be 2000 years, as suggested

by paleoseismic investigations (e.g., Ran et al., 2018). Note that clustering of earthquakes in time will affect the deformation pattern in interseismic periods (Meade & Hager, 2004), but we ignored this effect due to lack of evidences for earthquake clustering on the LMSF.

Based on the elastic material parameters obtained from seismic studies (Z. Zhang et al., 2010; Wang et al., 2007; Figure S1 in Supporting Information S1), we build layered structures on both sides of the LMSF following Diao et al. (2018). We further divide the lower crust beneath eastern Tibet into two parts to capture its lateral inhomogeneity as inferred by electrical resistivity and seismic velocity imaging (Bao et al., 2020; Zhao et al., 2012; Figure 1b). The lateral extension of the eastern part of the lower crust (D) is set to be a free parameter in the modeling (Figure S2 in Supporting Information S1). We utilize the Maxwell rheology body to model the long-term viscoelastic relaxation of the lower crust and upper mantle (Li et al., 2020). Initial tests indicate that the surface deformation is insensitive to the viscosity of the western lower crust (η_{lc}^{w}) beneath eastern Tibet and the viscosities of lower crust and upper mantle beneath the Sichuan Basin, which are fixed at 10^{18}, 10^{22}, and 10^{23} Pa·s, respectively (Diao et al., 2018; Huang et al., 2014; Shi & Cao, 2008). As a result, only the viscosities of the eastern lower crust (η_{lc}^{e}) and upper mantle (η_{um}) beneath eastern Tibet remain to be solved. After running the model for several earthquake cycles, the simulated ground velocities within each cycle become stable (Hetland & Hager, 2006; Savage & Prescott, 1978). Here, we take the average from decades of model predictions before the earthquake in the eleventh earthquake cycle to fit the observations. Note that, the effects induced by the fixed parameters (η_{lc}^{w} and T) are further tested and discussed in Section 4.1.

3.3. Grid Search Method

Under the VECD model and parameter settings described in Section 3.2, there are four free parameters in modeling the surface velocities: the shortening rate of Tibet to Sichuan Basin (v), the lateral extension of eastern lower crust (D) and the viscosities (η_{lc}^{e} and η_{um}) beneath eastern Tibet. Considering the non-linear relationship between the parameter and the ground velocity, we use a grid search method to obtain the optimal value of the parameter that best fits the observed vertical and horizontal velocities. Compared with horizontal component of surface deformation, the vertical component is more sensitive to the thrust movement (Wang & Tréhu, 2016). Therefore, we set the weights of the vertical and horizontal components to 0.75 and 0.25, respectively. As the tests shown in Figure S3 in Supporting Information S1, different weighting combinations (e.g., (0.60, 0.40) or (0.50, 0.50)) will not bias the solved optimal parameters. We then optimize these parameters by minimizing the misfit between the simulated velocities (V_{model}) and observed velocities (V_{obs}).

$$F\left(\eta_{lc}^{e}, \eta_{um}, v, D\right) = \mathrm{sqrt}\left(\sum_{j=1}^{N} \sigma_{j}^{-2}\left[V_{\mathrm{obs},j} - V_{\mathrm{model},j}\left(\eta_{lc}^{e}, \eta_{\mathrm{um}}, v, D\right)\right]^{2} / N\right), \tag{2}$$

where j is the index of the leveling and GPS site, and σ is the measurement error of the observed velocity. We further estimate the uncertainty of the parameter through the Monte Carlo method, and more details are described in Figure S4 in Supporting Information S1.

4. Results and Discussion

4.1. Results and Parameter Sensitivity Tests

Based on the VECD model, the optimal values of η_{lc}^{e}, η_{um}, v and D are estimated to be 1.0×10^{23}, 5.0×10^{20} Pa·s, 4.8 ± 0.4 mm/a and 200 km, respectively (Figures 2a–2f, S4 in Supporting Information S1). The inferred η_{lc}^{e} ($>10^{21}$ Pa·s) is about three orders of magnitude lager than that obtained by postseismic deformation studies (e.g., Diao et al., 2018; Huang et al., 2014). The corresponding range of η_{um} is constrained within $5.0 \times 10^{20-21}$ Pa · s, also higher than $\sim 10^{19}$ Pa·s inferred from postseismic studies (e.g., Huang et al., 2014; Wang et al., 2021). The optimal shortening rate (v) is higher than 0–3 mm/a obtained in many previous studies (e.g., Thatcher, 2007; Zheng et al., 2017) and lower than 5.7 ± 1.5 mm/a inferred by Thompson et al. (2015).

The optimal VECD model explains the leveling observation better than the elastic model, even though the estimated shortening rate of the elastic model (4.4 ± 0.4 mm/a) is close to that of the VECD model. The optimal VECD model predicts the detailed spatial feature of the leveling data in the far-field area (Figure 2g), whereas the elastic model fails to predict such spatial variation. For the horizontal GPS velocities, data-fittings are similar for

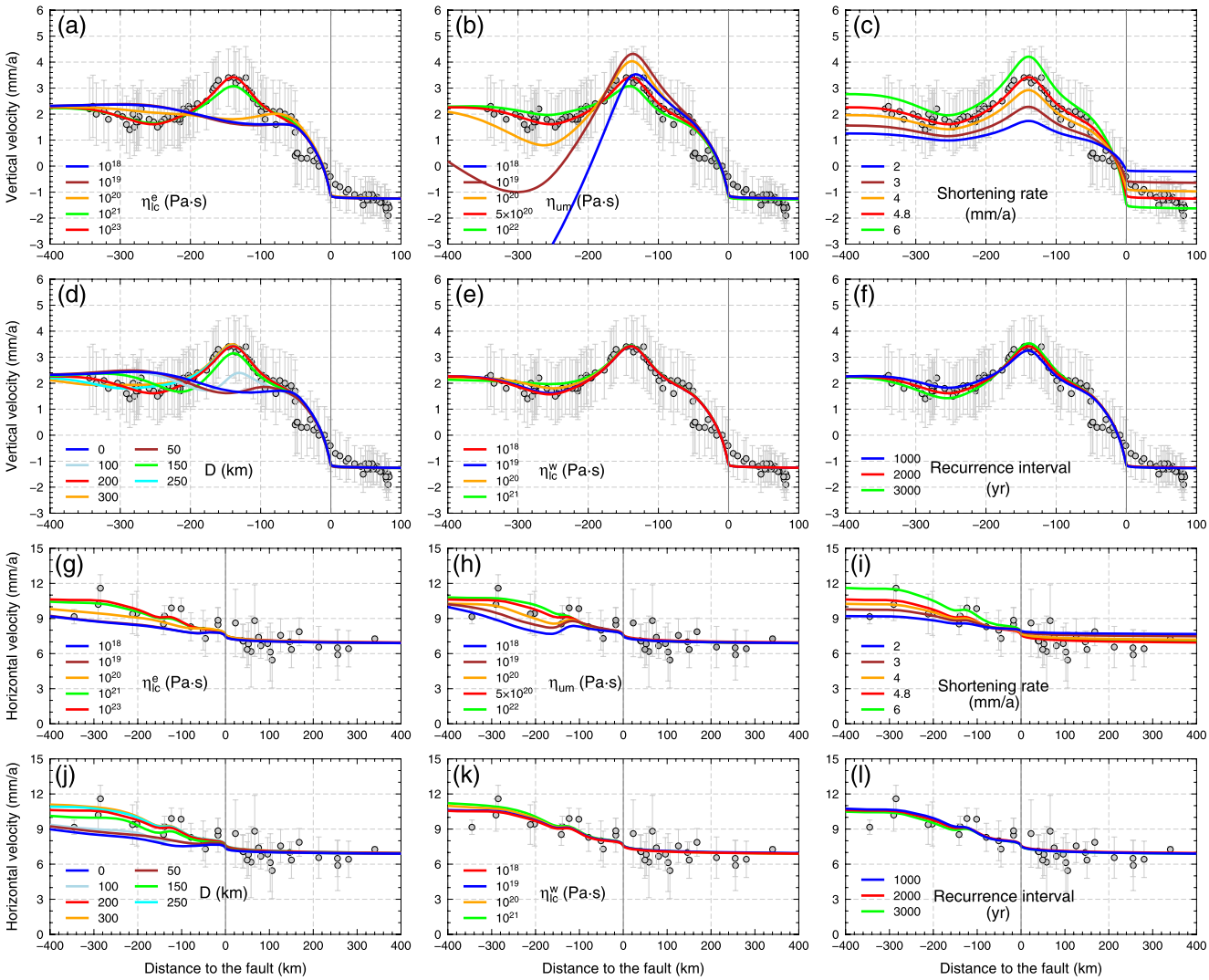

Figure 3. Sensitivity tests on model parameters. Comparisons of the simulated vertical and horizontal velocities obtained with different values of the target parameters, which are η^e_{lc} (a and g), η_{um} (b and h), v (c and i), D (d and j), η^w_{lc} (e and k), and T (f and l), respectively.

elastic and viscoelastic models (Figure 2h). In addition, we draw contributions of different deformation components in the optimal VECD model to better understand the earthquake-cycle deformation (Figure S5 in Supporting Information S1).

Based on the inferred optimal model, we perform additional tests to investigate the sensitivity of the observations to separate model parameters (Figure 3). For simplicity, we test one parameter each time and fix other parameters during the tests. We change the value of the target parameter within a reasonable range, and check the data-fittings of the predicted velocity curves to the observations. The modeling results indicate a sharp lower boundary of η^e_{lc} ($\sim 10^{21}$ Pa·s), and the models with lower values of this parameter fail to explain the leveling data (Figure 3a) due to the viscous subsidence effects (Figure S6 in Supporting Information S1). As shown in Figures 3b–3d, significant variations on data-fittings are observed when changing η_{um}, D or v, indicating that the observations have tight constraints on these parameters. By contrast, slight variations of velocity curves suggest that the observations are not sensitive to η^w_{lc} and T (Figures 3e and 3f). By further exploring the effects of thickness of the elastic layer (Table S1, Figures S7 and S8 in Supporting Information S1), fault geometry and locking degree (Figure S9 in Supporting Information S1) on modeling results, we find no essential changes on the estimations and the assigned values are reasonable in terms of data-fittings.

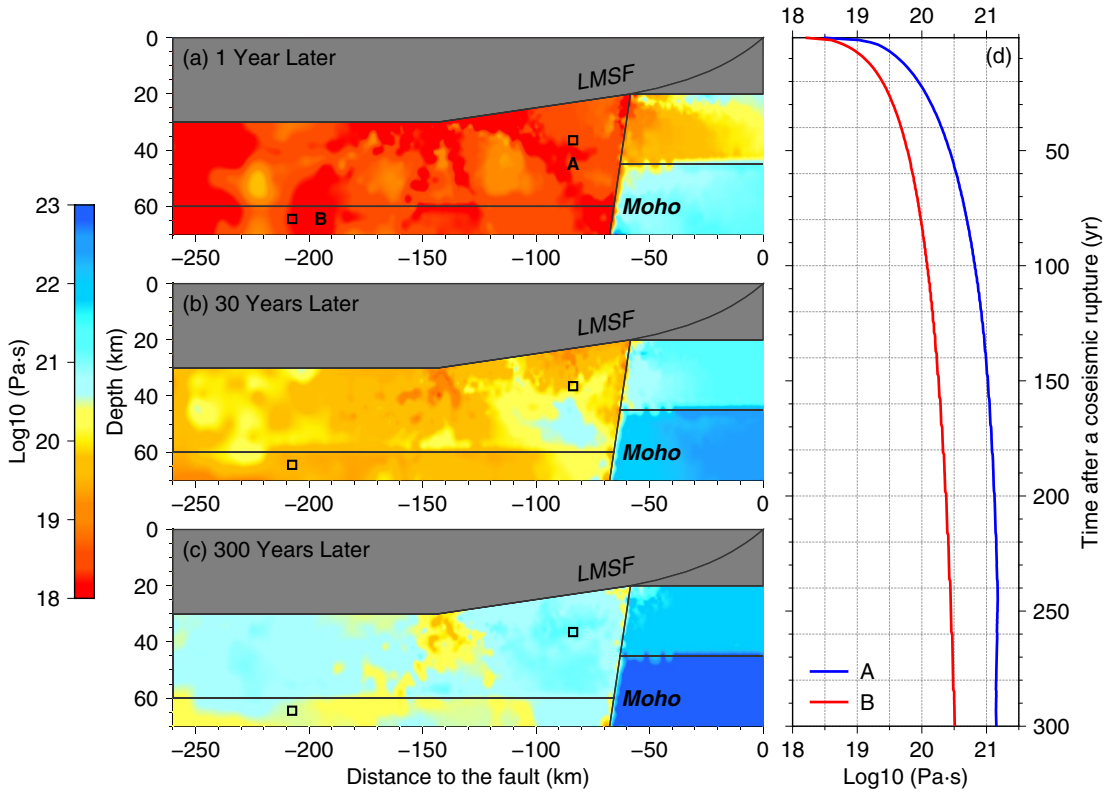

Figure 4. Calculated effective viscosity as a function of time after the Wenchuan earthquake, in a sub-region of the whole finite element model shown in Figure 1b and Figure S2 in Supporting Information S1. (a–c) show effective viscosities 1, 30 and 300 years after the earthquake, respectively. Viscosities are not shown in the upper crust (gray region), where the materials are assumed to be linearly elastic. (d) Temporal evolution of viscosity on two specific locations.

4.2. Rheological Structure Beneath the Longmen Shan Fault

Our study reveals a high-viscosity zone (>10^{21} Pa·s) in the lower crust beneath the eastern edge of Tibet, which is compatible with seismic tomography, magnetotelluric imaging and geological modeling evidence (Bao et al., 2020; Clark & Royden, 2000; Zhao et al., 2012). The lateral extension of the high-viscosity zone is estimated to be ~200 km, which agrees well with that of the high-velocity zone shown by seismic imaging (Bao et al., 2020). However, the inferred η^{e}_{lc} is obviously higher than ~10^{18} Pa·s obtained by previous postseismic studies (e.g., Diao et al., 2018; Huang et al., 2014). How to reconcile the discrepancy between these viscosities is crucial to understanding the rheological behavior.

We further explore the temporal evolution of viscosity in different periods with a power-law rheology inferred from laboratory experiments (Freed et al., 2006), for which the constitutive relation can be expressed by $\eta = C\sigma^{1-n}$ or $\dot{\varepsilon} = \sigma^{n}/2C$, where σ is differential stress, n is the power-law exponent, C is a power-law parameter associated with temperature and rock composition, and $\dot{\varepsilon}$ is strain rate. We compute the transient effective viscosity in postseismic periods as follows: (a) By combining a reasonable interseismic strain rate of 10^{-16} s^{-1} (Wang & Shen, 2020) with the interseismic viscosity from this study (Figure S10 in Supporting Information S1), we determine the preseismic differential stress by $\sigma_{pre} = 2\eta_{pre}\dot{\varepsilon}_{pre}$; (b) Then we obtain C by using $C = \eta_{pre}\sigma_{pre}^{n-1}$, where the power-law exponents (n) in the lower crust and upper mantle are assumed to be 3.1 and 3.5 (Afonso & Ranalli, 2004), respectively; (c) Based on the inferred C, we calculate the transient effective viscosity in postseismic periods using $\eta_{post} = \sigma_{post}/2\dot{\varepsilon}_{post}$ with a power-law viscoelastic model. As shown in Figure 4a, immediately after the Wenchuan earthquake (1 year), the stress in the materials around the fault is significantly enhanced, resulting in a low viscosity of ~10^{18} Pa·s in the lower crust. As the stress relaxes, the viscosity increases to ~10^{20} Pa·s 30 years later (Figure 4b), and after ~300 years the viscosity recovers to the interseismic level of ~10^{21} Pa·s (Figure 4c). Based on the results, we infer that the viscosity is highly depend on the stress state of the rock and shows a clear time-dependent behavior as stress relaxes during an earthquake cycle. This finding

may reconcile the discrepancies among viscosities inferred from postseismic deformation studies, geophysical imaging and geological modeling.

Combining with our results and that obtained by seismic/magnetotelluric imaging and geological modeling, we infer that the lower crust beneath the LMSF is of high strength to sustain the high topography on long-term time scales. However, under strong stress adjustment caused by coseismic ruptures, the strength of the lower crust shows transient reduction, leading to a significantly low effective viscosity. Therefore, the rheological parameters derived from transient postseismic deformation may not be used as the long-term strength of the lower crust or upper mantle (Freed & Bürgmann, 2004; Freed et al., 2006; Wang et al., 2012). The limited observations here cannot provide effective constraints on the rheological parameters of the western lower crust. However, seismic and magnetotelluric studies indicated a low viscosity zone of low seismic velocity and low resistivity beneath this area. Thus, the lower crustal viscosity may vary laterally beneath the eastern Tibetan Plateau.

4.3. Crustal Shortening Rate Across the Longmen Shan Fault

Most previous studies calculated the crustal shortening rate by directly differencing the relative motion between the eastern Tibetan Plateau and the Sichuan Basin (e.g., Shen et al., 2005; Zheng et al., 2017). These investigations simplified the fault geometry and neglected its effect, especially that induced by the detachment, which would underestimate the slip-deficit rate on the fault, leading to an overestimation of earthquake recurrence interval with the same moment magnitude. Thompson et al. (2015) considered the fault locking parameter and the geometrical variation, but they ignored the viscoelastic relaxation effects during earthquake cycles. Besides, most previous studies only relied on the horizontal GPS data, whereas the more sensitive vertical leveling data was not employed. In this study, both the horizontal and vertical observations are used in our viscoelastic model, allowing more reliable estimations on fault kinematic parameters. Note that, we use a single fault to represent the combined effect of sub-faults in the thrust system (Figure 1), and possible activity of small faults as suggested by the step in the vertical velocity profile (Figure 2g) was neglected.

In this study, we incorporate elastic and viscoelastic effects of crustal faulting during earthquake cycles, whereas the inelastic deformation associated with pervasive folds across the Longmen Shan was neglected. From spatial correlation among crustal shortening, structural relief, and topography shown by geological cross-sections, Hubbard and Shaw (2009) indicated that the crustal shortening plays a major role in uplift and topography of the Longman Shan. However, to what extent can this mechanism affect the present crustal deformation remains unclear. Relying on the potential correlation between long-term, inelastic vertical rate and short-term, interseismic vertical rate, Jolivet et al. (2020) found that 4%–8% of the geodetically derived interseismic vertical rates translate into permanent deformation in northern Chile. But similar correlations between short-term and long-term deformation are not necessarily observed worldwide (Jolivet et al., 2020). In the present case, the uplift toward the west of the Longmen Shan shows potential correlation with the topography, suggesting that part of the geodetically derived deformation may leak into topography building up. However, quantitative estimates on the percentage remain difficult and are beyond the scope of this study. The fast shortening rate obtained in this paper results in a faster strain accumulation process of the LMSF than most previous estimations, which may lead to shorter recurrence intervals or larger earthquakes than ever thought.

5. Conclusions

Based on the interseismic leveling and GPS observations, we investigate the lithospheric rheological structure and crustal shortening rate near the LMSF using viscoelastic deformation models. By incorporating the viscoelastic effects during earthquake cycles, the optimal model explains the observations better than the elastic model. The crustal shortening rate across the LMSF is estimated to be 4.8 ± 0.4 mm/a and the viscosity of upper mantle beneath eastern Tibet is constrained within $5.0 \times 10^{20-21}$ Pa·s. More importantly, we find a high-viscosity zone ($>10^{21}$ Pa·s) in the lower crust beneath the LMSF, where the steady-state viscosity is significantly higher than the transient viscosity inferred from previous postseismic studies. Further investigations with a power-law rheology suggest a clear stress-dependent behavior of the viscosity. Immediately after the Wenchuan earthquake, the effective lower crustal viscosity decreases to $\sim 10^{18}$ Pa·s under the coseismic stress loading, however, it increases with time as stress relaxes and finally recovers to the interseismic stable level ($\sim 10^{21}$ Pa·s). Our results highlight the

importance of viscoelastic effects on crustal deformation during earthquake cycles and clarify the stress-dependent behavior of the rheological structure beneath the LMSF.

Data Availability Statement

The GPS and leveling data used in this article were cited from Zheng et al. (2017) (https://doi.org/10.1002/2017JB014465) and Hao et al. (2014) (https://doi.org/10.1016/j.tecto.2014.06.016), respectively.

Acknowledgments
This work was supported by the National Natural Science Foundation of China (41731072) and the National Key R&D Program of China (2017YFC1500501). We thank T. Ben Thompson and one anonymous reviewer for valuable comments that highly improved the clarity of the paper, and editor Lucy M. Flesch for handling the manuscript. We thank Yashan Feng for polishing the paper. The figures were drawn using the Generic Mapping Tools software (Wessel & Smith, 1998).

References

Aagaard, B. T., Knepley, M. G., & Williams, C. A. (2013). A domain decomposition approach to implementing fault slip in finite-element models of quasi-static and dynamic crustal deformation. *Journal of Geophysical Research: Solid Earth*, *118*, 3059–3079. https://doi.org/10.1002/jgrb.50217

Afonso, J. C., & Ranalli, G. (2004). Crustal and mantle strengths in continental lithosphere: Is the jelly sandwich model obsolete? *Tectonophysics*, *394*(3–4), 221–232. https://doi.org/10.1016/j.tecto.2004.08.006

Bao, X., Song, X., Eaton, D. W., Xu, Y., & Chen, H. (2020). Episodic lithospheric deformation in eastern Tibet inferred from seismic anisotropy. *Geophysical Research Letters*, *47*(3), e2019GL08572. https://doi.org/10.1029/2019GL085721

Burchfiel, B. C., Royden, L. H., van der Hilst, R. D., Hager, B. H., Chen, Z., King, R. W., et al. (2008). A geological and geophysical context for the Wenchuan earthquake of 12 May 2008, Sichuan, People's Republic of China. *Geological Society of America Today*, *18*(7), 4–11. https://doi.org/10.1130/GSATG18A.1

Bürgmann, R., & Dresen, G. (2008). Rheology of the lower crust and upper mantle: Evidence from rock mechanics, geodesy, and field observations. *Annual Review of Earth and Planetary Sciences*, *36*(1), 531–567. https://doi.org/10.1146/annurev.earth.36.031207.124326

Chen, Z. H., Burchfiel, B. C., Liu, Y., King, R. W., Royden, L. H., Tang, W., et al. (2000). Global Positioning System measurements from eastern Tibet and their implications for India/Eurasia intercontinental deformation. *Journal of Geophysical Research*, *105*(B7), 16215–16227. https://doi.org/10.1029/2000JB900092

Clark, M. K., & Royden, L. H. (2000). Topographic ooze: Building the eastern margin of Tibet by lower crustal flow. *Geology*, *28*(8), 703–706. https://doi.org/10.1130/0091-7613(2000)28<703:TOBTEM>2.0.CO;2

Diao, F., Wang, R., Wang, Y., Xiong, X., & Walter, T. R. (2018). Fault behavior and lower crustal rheology inferred from the first seven years of postseismic GPS data after the 2008 Wenchuan earthquake. *Earth and Planetary Science Letters*, *495*, 202–212. https://doi.org/10.1016/j.epsl.2018.05.020

Diao, F., Wang, R., Zhu, Y., & Xiong, X. (2021). Revisiting the fault locking of the Central Himalayan Thrust with a viscoelastic earthquake-cycle deformation model. *Seismological Research Letters*, *93*(1), 193–200. https://doi.org/10.1785/0220200310

Diao, F., Xiong, X., Wang, R., Walter, T. R., Wang, Y., & Wang, K. (2019). Slip rate variation along the Kunlun fault (Tibet): Results from new GPS observations and a viscoelastic earthquake-cycle deformation model. *Geophysical Research Letters*, *46*(5), 2524–2533. https://doi.org/10.1029/2019GL081940

Freed, A. M., & Bürgmann, R. (2004). Evidence of power-law flow in the Mojave desert mantle. *Nature*, *430*(6999), 548–551. https://doi.org/10.1038/nature02784

Freed, A. M., Bürgmann, R., Calais, E., & Freymueller, J. (2006). Stress-dependent power-law flow in the upper mantle following the 2002 Denali, Alaska, earthquake. *Earth and Planetary Science Letters*, *252*(3–4), 481–489. https://doi.org/10.1016/j.epsl.2006.10.011

Hao, M., Wang, Q., Shen, Z., Cui, D., Ji, L., Li, Y., & Qin, S. (2014). Present day crustal vertical movement inferred from precise leveling data in eastern margin of Tibetan Plateau. *Tectonophysics*, *632*, 281–292. https://doi.org/10.1016/j.tecto.2014.06.016

Hetland, E. A., & Hager, B. H. (2006). Interseismic strain accumulation: Spin-up, cycle invariance, and irregular rupture sequences. *Geochemistry, Geophysics, Geosystems*, *7*(5), Q05004. https://doi.org/10.1029/2005GC001087

Huang, M. H., Bürgmann, R., & Freed, A. M. (2014). Probing the lithospheric rheology across the eastern margin of the Tibetan Plateau. *Earth and Planetary Science Letters*, *396*, 88–96. https://doi.org/10.1016/j.epsl.2014.04.003

Hubbard, J., & Shaw, J. H. (2009). Uplift of the Longmen Shan and Tibetan plateau, and the 2008 Wenchuan (M = 7.9) earthquake. *Nature*, *458*(7235), 194–197. https://doi.org/10.1038/nature07837

Jolivet, R., Simons, M., Duputel, Z., Olive, J. A., Bhat, H. S., & Bletery, Q. (2020). Interseismic loading of subduction megathrust drives long-term uplift in Northern Chile. *Geophysical Research Letters*, *47*(8), e2019GL085377. https://doi.org/10.1029/2019GL085377

Li, S., Fukuda, J. I., & Oncken, O. (2020). Geodetic evidence of time-dependent viscoelastic interseismic deformation driven by megathrust locking in the southwest Japan subduction zone. *Geophysical Research Letters*, *47*(4), e2019GL085551. https://doi.org/10.1029/2019GL085551

Liu, Q. Y., van der Hilst, R. D., Li, Y., Yao, H. J., Chen, J. H., Guo, B., et al. (2014). Eastward expansion of the Tibetan Plateau by crustal flow and strain partitioning across faults. *Nature Geoscience*, *7*(5), 361–365. https://doi.org/10.1038/ngeo2130

McCaffrey, R., Stein, S., & Freymueller, J. (2002). Crustal block rotations and plate coupling. *Plate Boundary Zones, Geodynamics Series*, *30*, 101–122. https://doi.org/10.1029/030GD06

Meade, B. J. (2007). Present-day kinematics at the India-Asia collision zone. *Geology*, *35*(1), 81–84. https://doi.org/10.1130/G22924A.1

Meade, B. J., & Hager, B. H. (2004). Viscoelastic deformation for a clustered earthquake cycle. *Geophysical Research Letters*, *31*(10), L10610. https://doi.org/10.1029/2004GL019643

Meade, B. J., & Hager, B. H. (2005). Block models of crustal motion in southern California constrained by GPS measurements. *Journal of Geophysical Research*, *110*, B03403. https://doi.org/10.1029/2004JB003209

Ran, Y. K., Wang, H., Chen, L. C., Chen, W. S., Lang, M. J., & Xu, X. W. (2018). Late-Quaternary fault activity of the Longmen Shan fault zone—Evidence from paleoseismic trenching. *Chinese Journal of Geophysics*, *61*(5), 1938–1948. https://doi.org/10.6038/cjg2018M0251

Reid, H. F. (1910). *The mechanics of the earthquake in the California earthquake of 18 April 1906*. In *Report* (Vol. 2). Carnegie Institute. Retrieved from https://ci.nii.ac.jp/naid/10017465191/

Savage, J. C. (1983). A dislocation model of strain accumulation and release at a subduction zone. *Journal of Geophysical Research*, *88*(B6), 4984–4996. https://doi.org/10.1029/JB088iB06p04984

Savage, J. C., & Prescott, W. H. (1978). Asthenosphere readjustment and the earthquake cycle. *Journal of Geophysical Research*, *83*(B7), 3369–3376. https://doi.org/10.1029/JB083iB07p03369

Shen, Z. K., Lü, J., Wang, M., & Bürgmann, R. (2005). Contemporary crustal deformation around the southeast borderland of the Tibetan Plateau. *Journal of Geophysical Research*, *110*, B11409. https://doi.org/10.1029/2004JB003421

Shen, Z. K., Sun, J., Zhang, P., Wan, Y., Wang, M., Bürgmann, R., et al. (2009). Slip maxima at fault junctions and rupturing of barriers during the 2008 Wenchuan earthquake. *Nature Geoscience*, *2*(10), 718–724. https://doi.org/10.1038/ngeo636

Shi, Y. L., & Cao, J. L. (2008). Lithosphere effective viscosity of continental China. *Earth Science Frontiers*, *15*(3), 82–95. https://doi.org/10.1016/S1872-5791(08)60064-0

Thatcher, W. (2007). Microplate model for the present-day deformation of Tibet. *Journal of Geophysical Research*, *112*, B01401. https://doi.org/10.1029/2005JB004244

Thompson, T. B., Plesch, A., Shaw, J. H., & Meade, B. J. (2015). Rapid slip-deficit rates at the eastern margin of the Tibetan plateau prior to the 2008 Mw 7.9 Wenchuan earthquake. *Geophysical Research Letters*, *42*(6), 1677–1684. https://doi.org/10.1002/2014GL062833

Wang, C. Y., Han, W. B., Wu, J. P., Lou, H., & Chan, W. W. (2007). Crustal structure beneath the eastern margin of the Tibetan Plateau and its tectonic implications. *Journal of Geophysical Research*, *112*, B07307. https://doi.org/10.1029/2005JB003873

Wang, K., Hu, Y., & He, J. (2012). Deformation cycles of subduction earthquakes in a viscoelastic Earth. *Nature*, *484*(7394), 327–332. https://doi.org/10.1038/nature11032

Wang, K., & Tréhu, A. M. (2016). Invited review paper: Some outstanding issues in the study of great megathrust earthquakes—the Cascadia example. *Journal of Geodynamics*, *98*, 1–18. https://doi.org/10.1016/j.jog.2016.03.010

Wang, M., & Shen, Z. (2020). Present-day crustal deformation of continental China derived from GPS and its tectonic implications. *Journal of Geophysical Research: Solid Earth*, *125*, e2019JB018774. https://doi.org/10.1029/2019JB018774

Wang, M., Shen, Z. K., Wang, Y., Bürgmann, R., Wang, F., Zhang, P. Z., et al. (2021). Postseismic deformation of the 2008 Wenchuan earthquake illuminates lithospheric rheological structure and dynamics of eastern Tibet. *Journal of Geophysical Research: Solid Earth*, *126*, e2021JB022399. https://doi.org/10.1029/2021JB022399

Wang, Q., Qiao, X., Lan, Q., Jeffrey, F., Yang, S., Xu, C., et al. (2011). Rupture of deep faults in the 2008 Wenchuan earthquake and uplift of the Longmen Shan. *Nature Geoscience*, *4*(9), 634–640. https://doi.org/10.1038/ngeo1210

Wessel, P., & Smith, W. H. F. (1998). New improved version of generic mapping Tools released. *Eos, Transactions American Geophysical Union*, *79*(47), 579. https://doi.org/10.1029/98EO00426

Xu, C., Liu, Y., Wen, Y., & Wang, R. (2010). Coseismic slip distribution of the 2008 Mw 7.9 Wenchuan earthquake from joint inversion of GPS and InSAR data. *Bulletin of the Seismological Society of America*, *100*(5B), 2736–2749. https://doi.org/10.1785/0120090253

Zhang, P. Z., Wen, X. Z., Shen, Z. K., & Chen, J. H. (2010). Oblique, high-angle, listric-reverse faulting and associated development of strain: The Wenchuan earthquake of May 12, 2008, Sichuan, China. *Annual Review of Earth and Planetary Sciences*, *38*(1), 353–382. https://doi.org/10.1146/annurev-earth-040809-152602

Zhang, Z., Yuan, X., Chen, Y., Tian, X., Kind, R., Li, X., & Teng, J. (2010). Seismic signature of the collision between the east Tibetan escape flow and the Sichuan Basin. *Earth and Planetary Science Letters*, *292*(3–4), 254–264. https://doi.org/10.1016/j.epsl.2010.01.046

Zhao, G., Unsworth, M. J., Zhan, Y., Wang, L., Chen, X., Jones, A. G., et al. (2012). Crustal structure and rheology of the Longmenshan and Wenchuan Mw 7.9 earthquake epicentral area from magnetotelluric data. *Geology*, *40*(12), 1139–1142. https://doi.org/10.1130/G33703.1

Zheng, G., Wang, H., Wright, T. J., Lou, Y., Zhang, R., Zhang, W., et al. (2017). Crustal deformation in the India-Eurasia collision zone from 25 years of GPS measurements. *Journal of Geophysical Research: Solid Earth*, *122*, 9290–9312. https://doi.org/10.1002/2017JB014465